Supplement for

The MISR Research Product Algorithm – Producing Global, Self-Consistent, Pixel-Level Aerosol Retrievals for the Multi-angle Imaging SpectroRadiometer

Michael Anstett [1,2], James A. Limbacher[3,4], and Ralph A. Kahn[5,6]

[1]Science Systems and Applications, Inc., Lanham MD 20706
[2]NASA Goddard Space Flight Center, Greenbelt MD 20771
[3]Science and Technology Corporation (STC), Hampton, VA
[4]National Oceanic and Atmospheric Administration, College Park MD 20740
[5]Laboratory for Atmospheric & Space Physics, University of Colorado Boulder, Boulder CO 80303
[6]Senior Research Scientist Emeritus, NASA Goddard Space Flight Center, Greenbelt MD 20771

Contents of this file

Introduction

This supplement contains a description of the MISR Research Product Algorithm (MRPA) over-land and over-water quality flags

Section S1.1 MRPA over-land quality flags

Validation for the MRPA is done using every available MISR-AERONET coincidence falling within the time windows specified in Section 2.4. MRPA quantities are averaged from results retrieved within 48 x 48-pixel (~53 km) boxes centered on the closest pixel to the AERONET site. As in previous versions, we establish a series of quality flags to mask out pixels where retrievals may be poor, such as in the presence of cloud, sea ice, or where retrieval fitting is poor (Limbacher et al., 2022). The following quality flags are used for over-land retrievals:

1. MISR surface height (from the MISR Ancillary Geographic Product (AGP) scene elevation dataset) is within 200m of the AERONET station height.
2. Scene-wide cosine of solar-zenith angle (mu0) is greater than 0.2.
3. At least seven of nine MISR cameras contain valid BRF data.
4. MISR pixels must be masked as land.
5. MISR prescribed (PSA) and retrieved (RSA) cost functions are both < 5.
6. MISR retrieved surface AOD < 9.
7. The normalized difference vegetation index (NDVI) using the prescribed surface albedo from MAIAC is > 0
8. Blue BRF max – blue BRF min (over all cameras) < 0.15 + 0.2 x exp(-1.0 x [MISR prescribed surface AOD]).
9. The MISR retrieved surface AOD standard deviation among all quality accepted (QA) pixels is < 1.
10. MISR pixels must be masked as clear from the interpolated MAIAC cloud mask.
11. MAIAC interpolated land mask must be defined and must not be masked as snow or ice

Quality flag 1 ensures that we are retrieving pixels from roughly within the same aerosol air mass, as aerosol properties can vary with height. Quality flag 2 ensures that the solar zenith angle is not so high as to cause issues such as surface shadowing. Quality flag 3 ensures we have enough "good" input multi-angle data for a high-quality retrieval. As we are validating land and water pixels separately, quality flag 4 establishes we are only including land retrievals in this section. Quality flag 5 screens out poor-quality retrievals, which are likely to be cloud. Similarly, with quality flag 6 we make the assumption that pixels with a combined surface AOD > 9 are most likely cloud contaminated. We introduce to the MRP the condition that NDVI from the MAIAC surface albedo (calculated as NDVI=(NIR-Red)/(NIR+Red)) must exceed 0.12, designed to include primarily dry and/or vegetated land. Quality flag 7 eliminates many high-brightness scenes such as over the Sahara, where the RSA struggles to constrain the surface, and issues of prescribing the surface to MISR using MODIS-MAIAC bands become especially significant. Ensuring NDVI is greater than zero can also eliminate unmasked water in the scene. Quality flag 8 masks partially cloudy MISR pixels, where clouds may be present in some cameras but not others. In such pixels, the difference between the minimum and maximum BRF will be quite large. Quality flag 9 applies a large-scale (low-frequency) variability filter to further exclude stray clouds. Quality flag 10 applies the interpolated MAIAC cloud mask described in Section 2.3. We additionally stipulate a few conditions on scene-wide basis:

1. AERONET site location is within ± 65 degrees latitude.
2. At least 10 pixels must be successfully retrieved using the pixel-level quality flags above.

Condition 1 eliminates sites in potentially snowy or ice-covered regions, and polar regions generally. Similarly, condition 2 stipulates the minimum solar zenith angle (corresponding to a zenith angle >~ 87°), below which retrieval results are very likely to be poor due to issues such as shadowing and extreme reflectance angles. Condition 3 aims to eliminate regions with persistent cloud or surface masking issues, by requiring each scene to contain at least ten quality-assessed pixels (out of 2304).

Section S1.2 MRPA over-water quality flags

For over-water validation, we use the same method as with the land retrieval, averaging 48 x48 pixel boxes over each AERONET site. We establish the following quality flags to identify good-quality retrievals, most continued from previous RA versions (Limbacher et al., 2022):

1. MISR surface height (from the MISR Ancillary Geographic Product (AGP) scene elevation dataset) is within 200m of the AERONET station height.
2. Scene-wide cosine of solar-zenith angle (mu0) is greater than 0.2.
3. At least seven of nine MISR cameras have valid BRF data.
4. MISR pixels must be masked as water (to exclude shoreline and ephemeral water from the MISR AGP surface feature ID).
5. The MISR-retrieved RSA surface cost function is < 5.
6. The MISR-prescribed surface AOD is < 9.
7. MISR BRF NDVI (minimized over all nine cameras) is < -0.075
8. N/A for over-water retrievals
9. (MISR prescribed surface AOD – MISR retrieved surface AOD) < (0.25 x MISR retrieved surface AOD + 0.05).
10. MISR pixels must be masked as clear from the interpolated MAIAC cloud mask.
11. MAIAC interpolated land mask must be defined and must not be masked as snow or ice

Quality flag 1 serves the same function as with the over-land retrieval. Similarly, quality flag 3 ensures we have enough "good" input data; this is especially important over water, where up to four cameras may be glint contaminated. Quality flag 4 ensures that a pixel is water, additionally eliminating pixels that may vary significantly in characteristic over MISR's lifetime. Quality flag 5 filters out poor-quality retrievals using the RSA's cost function, and Quality flag 6 helps eliminate cloud. Quality flag 7 also helps cloud masking, plus additional pixels containing ephemeral water or some land. Quality flag 8 is left over from the land retrievals, with no equivalent for over-water retrievals. Quality flag 9 aims to eliminate pixels contaminated by clouds or bright water, since the over-water PSA and RSA values should be similar in good-quality retrievals. Quality flag 10 applies a large-scale variability filter to eliminate any remaining clouds. Like in the over-land retrieval, quality flag 10 applies the interpolated MAIAC cloud mask. A minimum of 10 pixels in the scene must also have successful retrievals. We apply a rolling window to the land/water mask, stipulating that all pixels within a 5x5-pixel box must be masked as water. This eliminates river and ephemeral waterway retrievals where the surface characteristics may vary dramatically with time. As with the over-land analysis, we stipulate a few scene-wide conditions:

1. AERONET site location is within ± 60 degrees latitude.
2. At least 10 pixels must be successfully retrieved using the pixel-level quality flags above.

For the over-water retrieval, we specify a narrower latitude range than over land. This eliminates sites surrounded by freshwater bodies of water that may be frozen, with the basis for the flags remaining the same as for the over-land results.

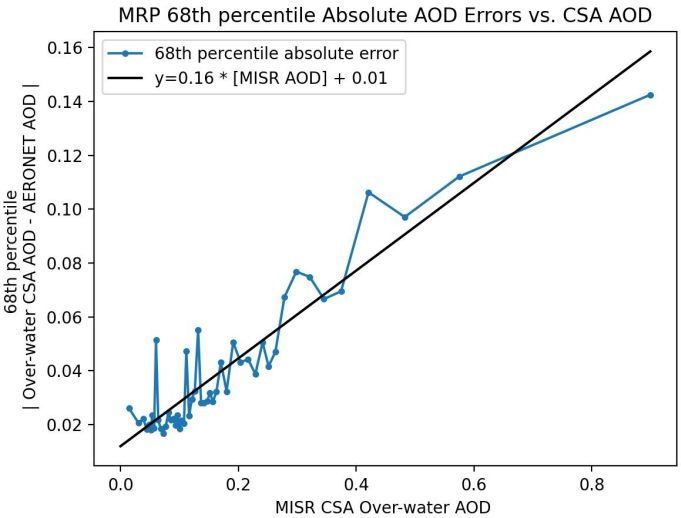

Figure S1: 68th percentile | CSA over-water 550nm AOD - AERONET 550nm AOD | error vs CSA AOD. Points are binned at 2% of total coincidences (roughly 588 coincidences per bin). The fit of these data is used to derive the expected over-water error of 0.16*(CSA AOD) + 0.01, which the black line represents.

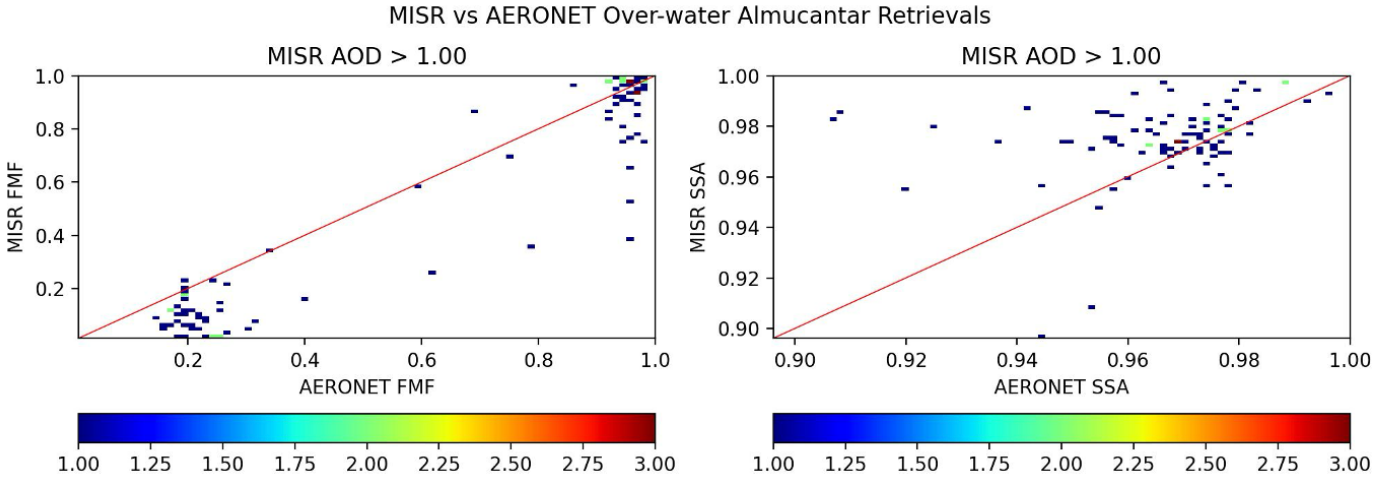

Figure S2: Plots of MISR CSA vs. AERONET 550nm over-water fine-mode AOD_{550} fraction (FMF) and 550 nm single-scattering-albedo (SSA). Plots correspond to results for AOD > 1.0. Results are plotted as 2D histograms, with the x and y axes representing AERONET and MISR results, respectively. Left to right, the columns of plots represent FMF and SSA. The embedded red lines represent one-to-one agreement between AERONET to MISR. Statistics associated with this figure are given in Table S8 below.

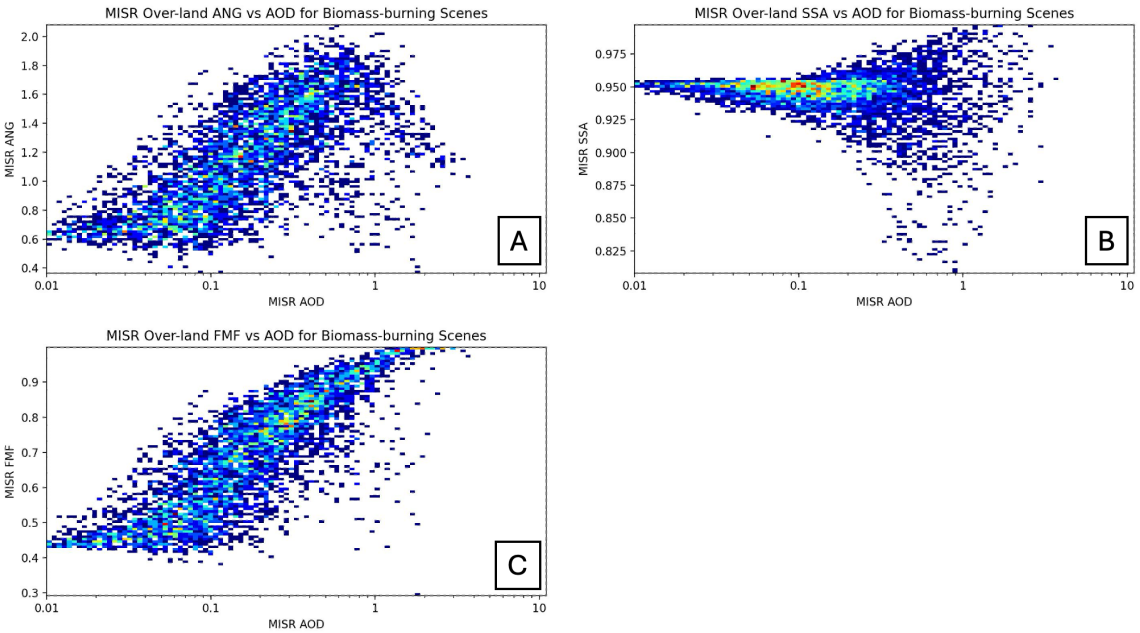

Figure S3: Plots of MISR CSA Ångström exponent (446-867nm), 550nm single-scattering-albedo (SSA) and fine-mode AOD_{550} fraction (FMF) vs 550nm AOD for over-land sites likely to contain biomass-burning source aerosols.

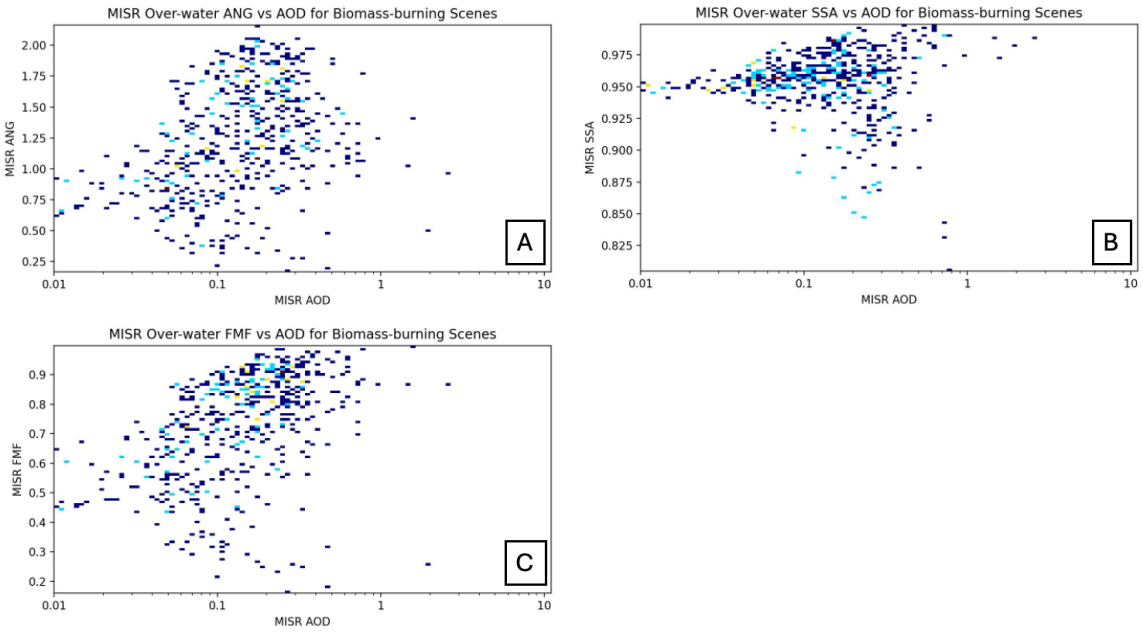

Figure S4: Plots of MISR CSA Ångström exponent (446-867nm), 550nm single-scattering-albedo (SSA) and fine-mode AOD_{550} fraction (FMF) vs 550nm AOD for over-water sites likely to contain biomass-burning source aerosols.

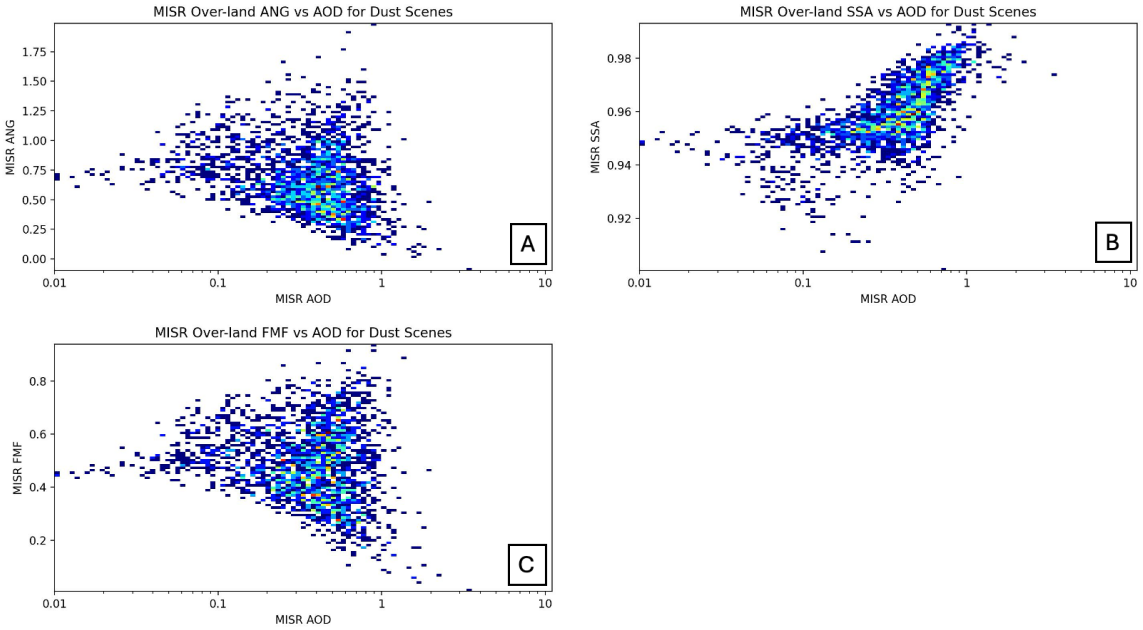

Figure S5: Plots of MISR CSA Ångström exponent (446-867nm), 550nm single-scattering-albedo (SSA) and fine-mode AOD_{550} fraction (FMF) vs 550nm AOD for over-land sites likely to contain dust source aerosols.

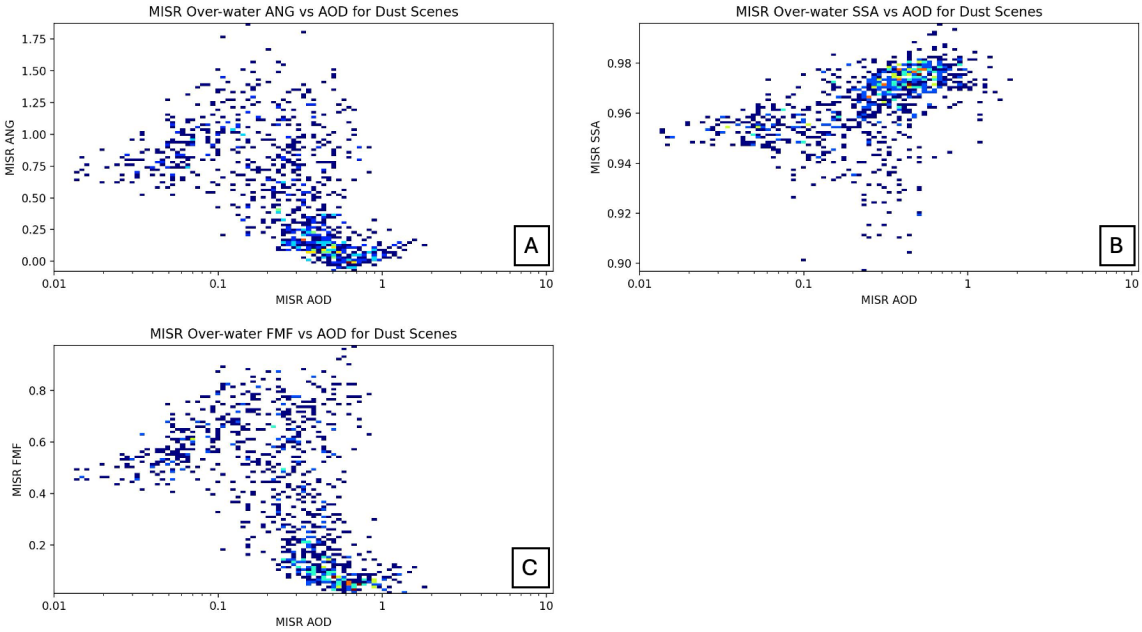

Figure S6: Plots of MISR CSA Ångström exponent (446-867nm), 550nm single-scattering-albedo (SSA) and fine-mode AOD_{550} fraction (FMF) vs 550nm AOD for over-water sites likely to contain dust source aerosols.

#	Analog (aerosol type)	r_0	r_1	r_c	w_c	r_e	ANG	SSA	AAE
1	Small, spherical, strongly absorbing BlS	0.001	0.75	0.06	1.70	0.12	1.80	0.80	1.34
2	Small, spherical, strongly absorbing BrS	0.001	0.75	0.06	1.70	0.12	2.04	0.80	3.02
3	Small, spherical, moderately absorbing BlS	0.001	0.75	0.06	1.70	0.12	2.05	0.90	1.37
4	Small, spherical, moderately absorbing BrS	0.001	0.75	0.06	1.70	0.12	2.18	0.90	3.14
5	Small-medium, spherical, strongly absorbing BlS	0.01	1.5	0.12	1.75	0.26	0.69	0.80	0.91
6	Small-medium, spherical, strongly absorbing BrS	0.01	1.5	0.12	1.75	0.26	0.76	0.80	2.36
7	Small-medium, spherical, moderately absorbing BlS	0.01	1.5	0.12	1.75	0.26	0.92	0.90	1.08
8	Small-medium, spherical, moderately absorbing BrS	0.01	1.5	0.12	1.75	0.26	0.98	0.90	2.74
9	Small, spherical, non-absorbing	0.001	0.75	0.06	1.70	0.12	2.31	1.00	N/A
10	Small-medium, spherical, non-absorbing	0.01	1.5	0.12	1.75	0.26	1.22	1.00	N/A
11	Medium, spherical, non-absorbing	0.01	5.0	0.24	1.80	0.57	0.21	1.00	N/A
12	Large, spherical, non-absorbing	0.1	10	0.50	1.85	1.28	-0.20	1.00	N/A
13	Very large, spherical, non-absorbing	0.1	50	1.00	1.90	2.80	-0.15	1.00	N/A
14	Small, non-spherical, very weakly absorbing	0.001	0.75	0.06	1.70	0.12	2.20	0.99	4.19
15	Small-medium, non-spherical, very weakly absorbing	0.01	1.5	0.12	1.75	0.26	1.03	0.99	3.93
16	Medium, non-spherical, very weakly absorbing	0.01	1.5	0.24	1.80	0.57	0.18	0.99	3.54
17	Very large, non-spherical, moderately absorbing	0.1	50	1.00	1.90	2.80	-0.08	0.94	2.67

Table S1: (From Limbacher et al., 2022) Microphysical and optical properties of the new RA aerosol component climatology. Column 1 represents the component number, column 2 describes the aerosol analogs, and columns 3–7 represent minimum radius, maximum radius, lognormal characteristic radius, lognormal characteristic width, and effective radius (respectively). Column 8 is the Ångström exponent (calculated using all four MISR bands at 446–867 nm), column 9 is 550 nm single-scattering albedo (SSA), and the last column is the

absorption Ångström exponent (AAE, calculated using all four MISR bands at 446–867 nm). Spherical aerosol component optical properties are modeled according to Mie theory, and all components are modeled with a lognormal particle size distribution. BlS corresponds to our black-smoke optical analogs, and BrS corresponds to our brown-smoke optical analogs. Red-colored rows correspond to models used only in the prescribed surface retrievals, whereas the one blue-colored row corresponds to the model only used by the retrieved surface aerosol retrieval. Purple-colored rows correspond to models used in both algorithms.

Table S2: Selected MRPA Validation Sites

Sites and timeframes were selected to be likely dominated by a particular aerosol type, which were then used to filter analysis of the MRPA. Tables specifying which sites and timeframes were used to filter the analysis follow. Each site is associated with a list of months, where each digit or character represents a month (where 1 refers to January 2 for February, etc., where O, N, and D refer to October, November, and December, respectively)

Table S2.1: Aeronet sites and months selected for likely biomass-burning-dominated scenes

Site_Name	Months	Key Aerosol Type	Site_Name	Months
Fort_McKay	678		Ibirapuera	45
Fort_McMurray	678		Sao_Paulo	45
Yellowknife	678		SP-EACH	45
Yellowknife_Aurora	678		Itajuba	45
Thompson	678		Cachoeira_Paulista	45
NSA_YJP_BOREAS	678		Asuncion_Airport	9
FLIN_FLON	678		Cordoba-CETT	9
CANDLE_LAKE	678		Pilar_Cordoba	9
Paddockwood	678		ARM_Cordoba	9
PRINCE_ALBERT	678		CEILAP-BA	34
Waskesiu	678		RdP-EsNM	34
OBS-SSA	678		CEILAP-UTN	34
SS_OJP_BOREAS	678		Montevideo_FING	34
Suffield	678		Palencia	D12
Univ_Of_Lethbridge	678		Valladolid_Sci	D12
Regina	678		Valladolid	D12
Bratts_Lake	678		Zaragoza	D12
Grand_Forks	678		Montsec	D12
Kelowna_UAS	9		CENER	D12
Kelowna_UAS	9		Pics_du_midi	D12
Saturn_Island	9		ASPET	D12
Lochiel	9		Biarritz	D12
Spokane	78		Momuy_MF	D12
Pinehurst_Idaho	78		Aire_Adour	D12

Pullman	78		Tarbes	D12
Rimrock	78		Tarbes_Etal	D12
Lewis-Clark_ID_USA	78		Le_Fauga	D12
Missoula_Pt_Six	78		TOULOUSE	D12
Missoula	78		Toulouse_MF	D12
Missoula_Midslope	78		Seysses	D12
Missoula_Waterworks	78		Strzyzow	D12
Missoula_Health_Dpt	78		CLUJ_UBB	8
McCall_Dragon_1	78		Timisoara	8
McCall_Dragon_2	78		Sofia_IEBAS	89
McCall_Dragon_3	78		Galata_Platform	89
McCall_Dragon_4	78		Eforie	89
McCall_Dragon_5	78		Baneasa	89
McCall_Dragon_6	78		Bucarest	89
McCall_Dragon_7	78		Bucharest_Inoe	89
Cliff_Creek_1	78		Magurele_Inoe	89
Cliff_Creek_2	78		Kyiv-AO	78
Cliff_Creek_3	78		Kyiv	78
Cliff_Creek_4	78		Yevpatoria	78
Cliff_Creek_5	78		Sevastopol	78
Cliff_Creek_6	78		Martova	789
TWRS	78		Donetsk	789
Taylor_Ranch_TWRS	78		Lugansk	789
Albany_Oregon	789		Moscow_MSU_MO	45
HjAndrews	789		Zvenigorod	45
White_Salmon	789		Yekaterinburg	345
NEON_WREF	789		Tomsk	345
Richland	78		Tomsk_22	345
Ukiah	78		Barnaul	345
PNNL	78		Krasnoyarsk	345
Bordman	78		Irkutsk	345
Trinidad_Head	6789		Yakutsk	678
Red_Bluff	6789		SONET_Harbin	34
Biggs	678		Ussuriysk	34
Univ_of_Nevada_Reno	678		Changchun	34
Tahoe_City	678		Liangning	34
McClellan_AFB	678		Baengnyeong	34
Sacramento_CARB	678		Soncheongcho	34
Modesto	678		Shijiazhuang-CHEY	6
NASA_Ames	678		SONET_Xingtai	6

San_Jose_State_Univ	678		Shijiazhuang-SZF	6
Moss_Landing	678		Xinglong	6
Marina	678		Yanqihu	6
Monterey	678		Beijing	6
Carmel_Valley	678		Lingshan_Mountain	6
NEON_SJER	678		Beijing_RADI	6
NEON17-SJER	678		Beijing_PKU	6
DRAGON_Madera_City	678		Beijing-CAMS	6
NEON_SoaprootSaddle	678		BEIJING_2002	6
NEON_TEAK	678		XiangHe	6
Fresno	678		PKU_PEK	6
Freson_2	678		Yufa_PEK	6
Fresno_X	678		Sonmiani	1
DRAGON_Clovis	678		Karachi	1
DRAGON_Drummond	678		Lahore	D
DRAGON_Parlier	678		Jaipur	9
DRAGON_Hanford	678		New_Delhi	9
DRAGON_Visalia	678		New_Delhi_IMD	9
DRAGON_Corcoran	678		IIT_Delhi	9
Angiola	678		Gual_Pahari	9
DRAGON_Huron	678		Amity_Univ_Gurgaon	9
Rogers_Dry_Lake	N		Pantnagar	59
ECCOE-Edwards_AFB	N		Nainital	59
UCSB	N		ARM_Nainital	59
Point_Mugu_Alpha	N		Vishkhapatnam	345
San_Nicolas_Island	N		Karunya_University	5
San_Nicolas	N		Dharwar	5
San_Nicolas_Vandal	N		Dibrugarh_Univ	D1
USC_SEAPRISM	N		Mandalay_MTU	34
USC_SEAPRISM	N		Mon_Pin	123
TABLE_MOUNTAIN_CA	N		Maeson	123
MISR-JPL	N		Fang	123
Mount_Wilson	N		Doi_Ang_Khang	123
Caltech	N		Chiang_Dao	123
Santa_Monica_Colg	N		Chiang_Mai_Met_Sta	123
UCLA	N		Doi_Inthanon	123
Yaqui	5		Omkoi	123
Monclova	34		Luang_Namtha	123
Tamihua	2		Son_La	123
T2_MAX_MEX	2345		Yen_Bai	123

T1_MAX_MEX	2345		Bac_Giang	123
T0_MAX_MEX	2345		NGHIA_DO	123
ORS_UNAM_ISNP	2345		Phu_Lien	123
Mexico_City	2345		Red_River_Delta	123
Orizaba	2345		BackGarden_GZ	12345
Veracruz_MAX_MEX	345		City_CZ	12345
Tuxtla_Gutierrez	5		Zhongshan_Univ	12345
Tenosique	5		Hong_Kong_Sheung	12345
UNC-Gaitan	D1		Hong_Kong_Hok_Tsui	12345
Balbina	78		Zhongshan	12345
ATTO-Campina	78		Kaiping	12345
Amazon_ATTO_Tower	78		Ubon_Ratchathani	D1
Manaus	78		Lopburi	D123
Manaus_EMBRAPA	78		Pimai	D123
ARM_Manacapuru	78		Silpakorn_Univ	D123
Sanatarem	78		Hua_Hin	D123
Belterra	78		Chulalaongkon	D123
UNC-Gaitan	D1		Bangkok	D123
Balbina	78		Chachoengsao	D123
ATTO-Campina	78		Sra_Kaeo	D123
Amazon_ATTO_Tower	78		Siem_Reap	D12
Manaus	78		Chi_Kraeng_Station	D12
Manaus_EMBRAPA	78		NhaTrang	D12
ARM_Manacapuru	78		Bac_Lieu	D12
Sanatarem	78		Vientiane	45
Belterra	78		Nong_Khai	45
Repressa_Samuel	78		ARM_Darwin	89O
Porto_Velho	78		Darwin	89O
Porto_Velho_UNIR	78		Jabiru	89O
Jamari	78		Lake_Argyle	5N
Ariquiums	789		Lucinda	N
Jaru_Reserve	789		Katibougou	ND
Jaru	789		IER_Cinzana	ND1
JARU_TOWN	789		Bondoukoui	ND1
Potosi_Mine	78		LAMTO-STATION	D12
Abracos_Hill	789		Koforidua_ANUC	D12
Ji_Parana_SE	789		Djouguo	D12
Ji_Parana_UNIR	789		ARM_DACCIWA_Save	D12
Ji_Parana	789		KITcube_Save	D12
Teles_Peres	789		Ilorin	D12

Alta_Floresta	789		CATUC_Bamenda	D12
Alta_Floresta_IF	789		Sao_Tome	D12
Agri_School	789		SEGC_Lope_Gabon	D12
Porto_Nacional	789		MUBFS	D12
Flor_De_Oro	789		Kibale	D12
LOS_FIEROS_98	789		AAU_Jackros_ET	D12
Los_Fieros	789		AAU_ET	D12
El_Refugio	9		Bujumbura	567
Concepcion	9		Misamfu	6789O
La_Paz	9		Kasama	6789O
Mount_Chacaltaya	9		Sakeji_School	679
El_Alto_Altiplano	9		Mwinilunga	679
Campo_Grande	9		Solwezi	679O
Campo_Grande_SONDA	9		Ndola	679O
GORDO_rest	D19		Mfuwe	679O
Cuiaba	D19		Niassa	9O
CAMPO_VERDE	D19		Zambezi	6789
CUIABA-MIRANDA	D19		Kaloma	6789
Chapada	D19		Kaoma	6789
Pantanal	D19		Mongu_Inn	6789
Etosha_Pan	678		Mongu	6789
Windpoort	678		Latoya	6789
Tsumkwe	678		Senanga	6789
Gorongosa	6789		Shesheke	9
Pietersburg	8ND			

155

Table S2.2: AERONET sites and months selected for likely dust-dominated scenes

Site_Name	Months		Site_Name	Months
Dahkla	456789O		Agoufou	456789O
Zouerate-Fennec	456789O		Homburi	456789O
Bordj_Dadji_Mokhar	456789O		Zinder_Airport	456789O
Tamanrasset_INM	456789O		Zinder_DMN	456789O
El_Farafa	456789O		Tamanrasset_TMP	456789O
Riyadh_Airport_SDSC	456789O		Qena_SVU	456789O
Solar_Village	456789O		Kuwait_Inst_Sci_Res	456789O
Hada_El-Sham	456789O		Shagaya_Park	456789O
KAUST_Campus	456789O		Kuwait_Airport	456789O
Rafha_Airport_SDSC	456789O		Hotan	456789O
Mezaira	456789O		Dunhuang	456789O

Hamim	456789O		Dunhuang_LZU	456789O
Bodele	456789O		HAMI	456789O
Dakar_Belair	456789O		Asia1	456789O
Bakar	456789O		Urumq	456789O
Bambey-ISRA	456789O		Minqin	456789O
Dalanzadgad	456789O		Jingtai	456789O
Inner_Mongolia	456789O		Yulin	456789O
Capo_Verde	456789O		Praia	456789O
Calhau	456789O		Tenerife	456789O
Roque_Muchachos	456789O		La_Palma	456789O
La_Laguna	456789O		Santa_Cruz_Tenerife	456789O
Izana	456789O		Teide	456789O
Las_Galletas	456789O			

Table S3: Comparison statistics of MISR 550nm over-land AOD against AERONET direct-sun 550nm AOD. Column 1 specifies which algorithm being compared against AERONET. For each algorithm, column 2 contains the number of coincidences used to compute the statistics. Column 3 contains the root mean squared error (RMSE), and column 4 displays mean Ångström error (MAE). Mean bias is displayed in column 4, with Pearson's correlation coefficient (r) in column 5. The full dataset associated with these statistics is plotted in Fig. 1 in the main text.

AOD Comparison	N	RMSE	MAE	Bias	r
RSA	69,191	0.092	0.028	0.005	0.930
PSA	69,191	0.152	0.073	0.088	0.881
CSA	69,191	0.083	0.028	0.008	0.941

Table S4: Statistics of over-land Ångström exponent comparison against AERONET corresponding to Fig. 2. The statistics of each algorithm are included, separating the rows. Column 1 specifies the CSA AOD threshold for each set of statistics. Column 2 contains the number of coincides for each statistic. Column 3 contains the root mean squared error (RMSE), and column 4 contains the median average error (MAE). Mean bias is reported in column 5, and Pearson's correlation coefficient (r) is reported in column 6. The full dataset associated with these statistics is plotted in Fig. 3 in the main text.

Retrieved-surface algorithm (RSA) ANG against AERONET					
AOD Threshold	N	RMSE	MAE	Bias	r
CSA AOD > 0.05	62651	0.428	0.280	-0.094	0.502
CSA AOD > 0.20	24436	0.338	0.221	0.058	0.759
CSA AOD > 0.50	5982	0.297	0.198	0.154	0.890
CSA AOD > 1.00	1127	0.284	0.167	0.041	0.850

Prescribed-surface algorithm (PSA) ANG against AERONET					
AOD Threshold	N	RMSE	MAE	Bias	r
CSA AOD > 0.05	62651	0.496	0.304	0.196	0.485
CSA AOD > 0.20	24436	0.497	0.289	0.295	0.667
CSA AOD > 0.50	5982	0.405	0.209	0.206	0.787
CSA AOD > 1.00	1127	0.269	0.142	-0.007	0.863
Combined-surface algorithm (CSA) ANG against AERONET					
AOD Threshold	N	RMSE	MAE	Bias	r
CSA AOD > 0.05	62651	0.429	0.280	-0.096	0.499
CSA AOD > 0.20	24436	0.337	0.219	0.055	0.760
CSA AOD > 0.50	5982	0.289	0.190	0.143	0.894
CSA AOD > 1.00	1127	0.252	0.147	0.004	0.884

Table S5: The statistics of over-land MISR particle properties vs AERONET inversion results, including fine-mode-fraction (FMF) and single-scattering albedo (SSA). Statistics are stratified by AOD threshold. For each set of statistics, N is the number of coincidences, r is the Pearson correlation coefficient, RMSE is the root mean squared error, MAE is median average error, and bias is the mean AERONET-MISR bias. The full dataset associated with these statistics is plotted in Fig. 4 in the main text.

1.0 < AOD < 10.0		
	FMF STATS	SSA STATS
N	795	795
r	0.913	0.679
RMSE	0.119	0.024
MAE	0.034	0.013
bias	0.034	0.006

Table S6: Comparison statistics of MISR 550nm over-water AOD against AERONET direct-sun 550nm AOD. Column 1 specifies which algorithm being compared against AERONET. For each algorithm, column 2 contains the number of coincidences used to compute the statistics. Column 3 contains the root mean squared error (RMSE), and column 4 displays mean Ångström error (MAE). Mean bias is displayed in column 4, with Pearson's correlation coefficient (r) in column 5. The full dataset associated with these statistics is plotted in Fig. 5 in the main text.

AOD Comparison	N	RMSE	MAE	Bias	r

RSA	26,256	0.063	0.023	0.007	0.931
PSA	26,256	0.083	0.040	0.044	0.925
CSA	26,256	0.063	0.023	0.009	0.932

Table S7: Statistics of over-water Ångström exponent comparison against AERONET corresponding to Fig. 2. The statistics of each algorithm are included, separating the rows. Column 1 specifies the CSA AOD threshold for each set of statistics. Column 2 contains the number of coincides for each statistic. Column 3 contains the root mean squared error (RMSE), and column 4 contains the median average error (MAE). Mean bias is reported in column 5, and Pearson's correlation coefficient (r) is reported in column 6. The full dataset associated with these statistics is plotted in Fig. 6 in the main text.

Retrieved-surface algorithm (RSA) ANG against AERONET					
AOD Threshold	N	RMSE	MAE	Bias	r
CSA AOD > 0.05	26478	0.367	0.226	0.050	0.708
CSA AOD > 0.20	8715	0.295	0.185	0.008	0.848
CSA AOD > 0.50	1331	0.288	0.186	-0.169	0.917
CSA AOD > 1.00	159	0.311	0.186	-0.210	0.913
Prescribed-surface algorithm (PSA) ANG against AERONET					
AOD Threshold	N	RMSE	MAE	Bias	r
CSA AOD > 0.05	26478	0.533	0.286	0.222	0.566
CSA AOD > 0.20	8715	0.396	0.203	0.187	0.806
CSA AOD > 0.50	1331	0.308	0.160	0.116	0.880
CSA AOD > 1.00	159	0.275	0.152	0.074	0.882
Combined-surface algorithm (CSA) ANG against AERONET					
AOD Threshold	N	RMSE	MAE	Bias	r
CSA AOD > 0.05	26478	0.366	0.225	0.051	0.708
CSA AOD > 0.20	8715	0.293	0.182	0.012	0.849
CSA AOD > 0.50	1331	0.273	0.168	-0.142	0.916
CSA AOD > 1.00	159	0.228	0.106	-0.047	0.918

Table S8: The statistics of over-water MISR particle properties vs AERONET inversion results, including fine-mode-fraction (FMF) and single-scattering albedo (SSA). Statistics are stratified by AOD threshold. For each set of statistics, N is the number of

coincidences, r is the Pearson correlation coefficient, RMSE is the root mean squared error, MAE is median average error, and bias is the mean AERONET-MISR bias. The full dataset associated with these statistics is plotted in Fig. S2 above.

1.0 < AOD < 10.0		
	FMF STATS	SSA STATS
N	90	90
r	0.956	0.273
RMSE	0.150	0.020
MAE	0.062	0.008
bias	-0.088	0.009

References

Limbacher, J.A., R.A. Kahn, and J. Lee, 2022. The New MISR Research Aerosol Retrieval Algorithm: A Multi-Angle, Multi-Spectral, Bounded-Variable Least Squares Retrieval of Aerosol and Surface Properties. *Atmosph. Meas. Tech. 15, 6865–6887,* doi:10.5194/amt-15-6865-2022.